JOURNAL OF GEOPHYSICAL RESEARCH, VOL. 104, NO. E10, PAGES 24,195–24,210, OCTOBER 25, 1999

Quantitative compositional analysis using thermal emission spectroscopy: Application to igneous and metamorphic rocks

Kimberly C. Feely and Philip R. Christensen
Department of Geology, Arizona State University, Tempe

Abstract. The mineral composition of a suite of igneous and metamorphic rocks was determined using the thermal infrared emission spectra of these rocks in a linear spectral deconvolution algorithm. This algorithm assumes that the infrared spectrum of each rock is a linear mixture of the component mineral spectra weighted by volume abundance. A diverse suite of 36 common rock-forming and accessory minerals was used in the deconvolution. The model was tested by comparing the mineralogy derived from the infrared spectrum with petrographically estimated abundances for 45 igneous and 51 metamorphic rock samples. The mineral abundances derived from these two techniques agree to within ±7–15% for the primary minerals feldspar, pyroxene, quartz, and calcite/dolomite and ±9–17% for secondary minerals such as micas and amphiboles. These differences are comparable to the error for traditional thin section mode estimates, which are ±5–15% for major minerals and ≤5% for minor minerals. The detection limit for the primary and secondary minerals found in the rocks analyzed ranged from 5 to 10%. Each major rock type studied here was easily distinguished by its spectral characteristics. The best results, in both the qualitative determination of the rock type and dominant minerals and the quantitative reproduction of absorption features and mineral composition, were obtained for igneous rock samples. For metamorphic rocks, pelite and quartzo-feldspathic samples gave slightly better results than calcareous or mafic samples. A controlled analysis, in which the end-member suite was reduced based on an initial estimate of the rock type, only improved the results by several percent for most primary and secondary minerals. The quality of the obtained results demonstrates that a linear deconvolution of infrared emission spectra provides an accurate, rapid technique for determining the quantitative mineral composition of rock samples in a laboratory and has application to future in situ measurements.

1. Introduction

Thermal infrared vibrational spectroscopy is based on the principle that vibrational motions occur within a crystal lattice at fundamental frequencies that are directly related to the crystal structure and elemental composition (i.e., mineralogy) [e.g., *Wilson et al*., 1955; *Farmer*, 1974]. The fundamental frequencies of geologic materials typically correspond to wavelengths greater than ~6 μm and provide a diagnostic tool for identifying virtually all commonly occurring minerals. Although infrared (IR) spectroscopy has been extensively used in chemistry and physics for over a century, only relatively recently has this technique been applied to the qualitative and quantitative analysis of geologic materials. Laboratory studies have demonstrated that absorption features in an infrared spectrum of a mineral vary systematically with composition and crystal structure and have characterized the spectra of individual minerals [e.g., *Lyon*, 1965; *Walter and Salisbury*, 1989; *Salisbury et al*., 1991; *Salisbury*, 1993]. Several studies have examined the infrared spectra of mixtures of particulate minerals and have shown that these mixtures can be reproduced by the linear combination of infrared spectra [*Thomson and Salisbury*, 1993; *Ramsey and Christensen*, 1998]. However, there have been few attempts to quantitatively determine the mineral composition of rocks using spectroscopic methods.

Notable first attempts to extract a rock composition from an infrared spectrum of a crushed or powdered sample were conducted by *Hunt and Turner* [1953] and *Lyon et al*. [1959]; both studies were able to quantify the presence of primary minerals with ±10% and ±5% accuracy, respectively. Further infrared spectroscopic work by Lyon, with various collaborators, developed three important new hypotheses. First, spectral effects caused by preferential orientation of minerals are mainly a concern for foliated metamorphic rocks, as minerals in most igneous rocks are randomly oriented [*Lyon and Burns*, 1963]. Second, the wavelength positions of the fundamental absorption bands are not strongly affected by grain size [*Lyon*, 1963]. Third, the combined set of peaks and troughs composing a spectrum is diagnostic of the qualitative bulk composition of the rock [*Lyon*, 1963], and the depth of the peaks and troughs is important to the quantitative modal composition of the rock [*Lyon and Burns*, 1963; *Lyon*, 1963].

The next advance in the spectroscopic analysis of geologic materials occurred when it was shown that laboratory emission measurements could be made directly from the rough surfaces of rock samples [*Lyon*, 1965]. Emission measurements had not been made previously due to the difficulty in accurately determining the temperature of the rock sample. Lyon made the crucial assumption that the absolute temperature of the sample was not necessary as long as it could be reproduced by a

Paper number 1999JE001034.
0148-0227/99/1999JE001034$09.00

blackbody standard. Another conclusion from his work was that high surface porosity, roughness, or particle sizes <50–100 μm cause decreases in feature depth significant enough to make the analysis of emission spectra the most difficult of the infrared techniques.

Lyon [1965] showed that the distinctive reststrahlen bands (emissivity minima) due to the fundamental silicon-oxygen stretching modes in the silicate lattice shift to longer wavelengths with decreasing silica content in igneous rocks. Other approaches have been developed to use spectral shape to determine bulk composition [*Vincent and Thompson*, 1972; *Walter and Salisbury*, 1989]. Application of these techniques allows interpretation of chemical composition from the spectrum but does not achieve the ultimate goal of determining the mineral composition directly from a measured spectrum.

The simplest approach to calculating a modal analysis from an infrared spectrum is based on the assumption that the spectrum of a mixture, such as that of a rock, is a linear combination of the spectra of its component minerals. *Adams et al*. [1986] performed the first "reverse sense" application of the linear mixing hypothesis when they identified four components in the multispectral images obtained at the Viking Lander 1 site and used these as end-member components in a least squares fitting method to analyze the composition of the scene. *Thomson and Salisbury* [1993] provided laboratory verification of the hypothesis in the "forward sense" by measuring reflectance spectra of granular mineral mixtures of various proportions and comparing these spectra with spectra of mixtures synthesized from weighted proportions of the individual mineral spectra. Most recently, *Ramsey and Christensen* [1998] performed a reverse sense application of linear mixing on granular mineral mixtures and developed an algorithm for identifying the components in a mixed infrared emission spectrum. Statistical analyses performed in these studies indicate that the abundances of minerals in these simple mixtures are predictable to within $\pm 5\%$.

The purpose of the work presented here is to apply a linear deconvolution model to measured thermal infrared emission spectra of igneous and metamorphic rocks in order to determine the quantitative mineral composition of the samples. These models can be applied to laboratory sample analyses, terrestrial remote sensing observations, and future in situ field sample analysis.

2. Approach

2.1. Modal Analysis by Deconvolution

Previous studies have demonstrated that the infrared spectra of mixtures of granular materials are closely approximated by the linear combination of the component spectra and that the fraction of each component in the spectrum closely matches the volume abundance of each component in the sample [*Ramsey and Christensen*, 1998; *Thomson and Salisbury*, 1993]. The linear nature of the mixing of infrared spectra is due primarily to the high absorption coefficients of vibrational absorptions, which minimize transmission through grains and reduces multiple-grain interactions. Several linear retrieval (deconvolution) models have been developed to determine the mineral abundance from an infrared spectrum [*Adams et al*., 1986; *Johnson et al*., 1992; *Ramsey and Christensen*, 1998]. In this paper we have used the specific linear deconvolution algorithm developed by *Ramsey and Christensen* [1998]. The inputs to this algorithm are a mixed spectrum and a suite of end-member mineral spectra; the results are a best fit model of the mixed spectrum, a list of the end-members present and their volume percentages, and a determination of the error of the model.

Deconvolution is achieved using matrix algebra to solve a system of equations, created from the rock and mineral spectra, by minimizing the residual error to produce a best fit solution [*Adams et al*., 1986; *Johnson et al*., 1992; *Ramsey and Christensen*, 1998]. End-member mineral spectra are used to create the matrix $[X]_{(\lambda,\eta)}$ where λ is the number of wavelengths in the end-member spectra and η is the number of end-members; for most cases in this study, λ was 500–600 and η was 25–40. Thus the matrix component $[X]_{(i,j)}$ is the value of the emissivity at the ith wavelength of the jth end-member mineral. Emissivity values of the mixed (rock) spectrum are written into a column vector $[U]_{(\lambda)}$, and the percentage that each end-member contributes to the model is given in the "solution vector" $[\zeta]_{(\eta)}$, in which each of the elements must sum to 1.0 $\pm$ a small error. For this application the values of the solution vector are the derived modal abundances of the sample.

In the linear deconvolution model [*Adams et al*., 1986; *Johnson et al*., 1992; *Ramsey and Christensen*, 1998] the equation describing how the end-member minerals are related to the mixed rock spectra is

$$[X]_{(\lambda,\eta)}[\zeta]_{(\eta)} = [U]_{(\lambda)}, \tag{1}$$

which can be solved for the end-member percentages $[\zeta]_{(\eta)}$, giving

$$[\zeta]_{(\eta)} = ([X]^T_{(\eta,\lambda)}[X]_{(\lambda,\eta)})^{-1}[X]^T_{(\eta,\lambda)}[U]_{(\lambda)}. \tag{2}$$

Because λ is greater than η, the solution is overdetermined, and the single model which best fits the available data must be identified. Selection of a best fitting model is accomplished by simultaneously calculating and minimizing a linear least squares fit from the difference of the measured emissivity (ε_i) and the modeled emissivity ($\Sigma X_j\zeta_j$) created from all end-members $j = 1$ through η, inversely weighted by the uncertainty in the spectral measurement at each wavelength, σ_i, giving

$$\chi^2 = \sum_{i=1}^{\lambda} \left(\frac{\varepsilon_i - \sum_{j=1}^{\eta} X_j\zeta_j}{\sigma_i} \right)^2. \tag{3}$$

To minimize the chi-square (χ^2) equation and produce the best fitting model, end-members and corresponding percentages are chosen such that the derivative of (3), taken with respect to $[\zeta]_{(j)}$, is equal to zero.

Included with the model results is the error indicating how well the model reproduces the original mixed spectrum. The residual error at each wavelength, $\delta(i)$, is calculated from the difference between the measured and modeled emissivities. To give a single error value to the entire fit, the residual error is summed over all wavelengths in the root-mean-square (RMS) error equation:

$$\mathrm{RMS} = \sqrt{\sum_{i=1}^{\lambda} \delta_i^2/\lambda}. \tag{4}$$

Values of $[\zeta]_{(\eta)}$ are mathematically allowed to be negative in order to improve the model fit to the data. However, negative

abundances have no physical meaning and are not allowed in the final solution. This restriction was achieved by removing end-members that contribute negative percentages to the model during the first iteration, recalculating the model with the remaining end-members, and continuing this process until all percentage values were positive.

2.2. Rock Sample Selection

A representative suite of 96 igneous and metamorphic rock samples was selected from various collections at Arizona State University (ASU) for this study. Samples were chosen that conformed to two criteria: (1) Each sample had compositional and physical properties (grain size, texture, etc.) that are representative of its rock type. Although unusual characteristics often provide a more interesting study, simplicity is a more desirable quality to establish confidence in the technique. (2) Each sample had been studied previously by traditional petrographic techniques, and modal abundances had been calculated. The petrographically determined modes, hereinafter referred to as the "known" modes, were used as a basis of comparison for establishing the accuracy of the spectral deconvolution.

Rock samples used in this study include 26 granitic igneous rocks, 8 rhyolitic to andesitic igneous rocks, 11 andesitic to basaltic igneous rocks, 19 pelitic metamorphic rocks, 9 calcareous metamorphic rocks, 13 mafic metamorphic rocks, and 10 quartzo-feldspathic metamorphic rocks. Each sample is relatively large, up to 10 cm in diameter, allowing the rocks to be measured in their natural state, i.e., not crushed or powdered. Detailed descriptions of each rock sample, including a brief physical, petrographic, and mineralogical description, known modal abundances with a description of the technique used, associated errors, references, and a measured infrared spectrum, are available from *Feely* [1997].

Spectra of the rock samples were obtained at 2 cm^{-1} sampling over $\approx$1600–400 cm^{-1} ($\approx$6–25 μm) using an instrument that has two main components: a commercial Mattson-Cygnus 100 spectrometer and a custom external sample chamber. The main body is a Michelson interferometric spectrometer that has been modified to collect infrared energy emitted from a sample source. A Plexiglas glovebox, adjacent to the external port of the spectrometer, houses the sample chamber and the mirrors that direct the sample energy into the optical path of the spectrometer. Constant environmental conditions within the sample chamber were obtained by insulating the chamber with a double-walled cylinder containing circulating water at a controlled temperature of 24.0°C $\pm$ 0.03 [*Ruff et al*., 1997]. This chamber approximates a blackbody cavity, allowing only sample energy and interior reflected energy (removed during calibration) out to the detector through an opening on the chamber top. To reduce the effects of variable atmospheric conditions in the laboratory, the glovebox and spectrometer were purged continuously with "scrubbed air," free of particulates, CO_2, and water vapor, and also purged during spectra acquisition with N_2 gas. See *Ruff et al*. [1997] for a more detailed description of the spectrometer apparatus and spectral measurement procedures.

Rock samples were heated in an oven at 80°C for ~24 hours in order to increase the signal-to-noise ratio. Hot samples were then placed inside an insulated sample cup and enclosed in the sample chamber. Depending on the height of the sample within the chamber, the diameter of the spot viewed by the spectrometer can be varied from ~1.5 to 5.0 cm in order to optimize the available surface area of the sample. This spot size was adjusted to account for variations in sample size and to maximize the number of mineral grains observed. During a 7-min acquisition period, 260 interferograms were collected per sample spot and averaged together to produce the final spectrum.

Calibration of the raw spectrum to emissivity was achieved using two calibrated blackbodies [*Christensen and Harrison*, 1993; *Ruff et al*., 1997]. Spectra were obtained from the two blackbodies, a "warm" 70°C source and a "hot" 100°C source, using the same conditions and methods described above for rocks. Measurement of the warm blackbody was repeated at least once every hour. Emissivity of the sample ($\varepsilon_{samp}(\lambda)$) was calculated as a function of wavelength from the equation given by *Christensen and Harrison* [1993]:

$$\varepsilon_{samp}(\lambda) = \frac{\frac{V_{meas}(\lambda, T)}{F} - B_{env}(\lambda, T) + B_{inst}(\lambda, T)}{B_{samp}(\lambda, T) - B_{env}(\lambda, T)}, \quad (5)$$

where $V_{meas}(\lambda, T)$ is the voltage measured by the instrument, F is the instrument response function calculated from the two blackbodies, $B_{env}(\lambda, T)$ is the radiance of the environment estimated by a Planck curve at the sample chamber temperature, $B_{inst}(\lambda, T)$ is the radiance of the instrument estimated by a Planck curve at the instrument temperature, and $B_{samp}(\lambda, T)$ is the radiance of the sample estimated by a Planck curve at the calculated sample brightness temperature. Sample emissivity values measured and calculated as described above are accurate in most cases to within 2% and reproducible to better than 1% [*Ruff et al*., 1997].

The measured spectra shown throughout this paper were produced from the calibrated emissivity with some additional processing. First, in an attempt to get the most representative spectrum of each rock sample, three to four spots from rough and cut surfaces were measured for each sample and averaged together. For metamorphic samples, emissivity measurements of most samples represent the combination of views both normal and parallel to the foliation direction. Second, sharp (two to five samples wide) spikes in the spectra at 1221, 845, and 667 cm^{-1} occur due to known instrument noise and CO_2 and were removed by interpolation.

2.3. End-Member Minerals

The fundamental assumption in this work is that all of the minerals present in each rock are contained in the end-member mineral suite used in the deconvolution. The accuracy of the deconvolution modal analysis technique for identifying solid-solution mineral constituents is dependent upon having end-members available with the correct structure and composition [*Ramsey and Christensen*, 1998; *Hamilton et al*., 1997]. The Arizona State University (ASU) Mineral Library currently contains spectra of ~160 minerals, carefully selected for compositional purity, with detailed information on the composition, physical condition, history, and quality of each mineral [*Christensen et al*., 1999]. Most library minerals are granular samples, with sizes ranging from 710 to 1000 μm, and have spectra obtained using methods similar to those described above. It has been shown [*Ramsey and Christensen*, 1998] that use of mineral end-members in this size range is appropriate for deconvolution of solid samples and avoids nonlinear complications due to scattering effects [*Conel*, 1969; *Hunt and Vincent*, 1968].

Table 1. End-Member Mineral Suites Used in Deconvolution

TES Mineral Library Number	Mineral	Blind Application, % Strength of Spectrum	Controlled Application, % Strength of Spectrum
	amphiboles		
HS-116.4B	actinolite	100	
BUR-4760	anthophyllite	100	
WAR-0404	hornblende	100	100
BUR-840	biotite	55	55
BUR-1100F	calcite	100	100
WAR-1924	chlorite	100	100
BUR-1840C	dolomite	100	
BUR-1940	epidote	100	100
	feldspars		
BUR-3460A	microcline	100	100
WAR-RGSAN01	orthoclase	100	100
(Sanidine.1s)	sanidine*	45	45
WAR-0235	albite	100	100
WAR-0024	andesine	100	100
BUR-340	anorthite	100	100
BUR-3080A	labradorite	100	100
WAR-0234	oligoclase	100	100
BUR-120A	garnet	100	
(ODG-95)	glass - obsidian†	100	100
WAR-0219	glaucophane	100	
WAR-1002	kyanite	100	
WAR-5474	muscovite	80	80
FAY-01	olivine - fayalite	100	100
BUR-3720	olivine - forsterite	100	100
HS-23.3B	phlogopite	100	
	pyroxenes		
WAR-6474	augite (CPX)	100	100
BUR-1820	diopside (CPX)	100	100
WAR-5780	diopside (CPX)	100	100
NMNH-93527	bronzite (OPX)	100	100
NMNH-R1440	enstatite (OPX)	100	100
BUR-5080	wollastonite	100	
BUR-4120	quartz	100	100
(no number)	quartz slab	100	100
HS-8.4B	serpentine	200	200
BUR-4640C	talc	280	
(Vesuvian.1s)	vesuvianite*	100	
(Zoisite.1c)	zoisite*	250	
	blackbody	100	100

Total number of end-members is 37 for the blind application and 26 for the controlled application. CPX, clinopyroxene; OPX, orthopyroxene.

* Mineral spectrum obtained from *Salisbury et al*. [1991].

† End-member spectrum obtained from *Ramsey et al*. [1993].

A suite of 36 minerals (Table 1) commonly found as primary, secondary, or accessory minerals in igneous and metamorphic rocks was assembled for use in the deconvolution algorithm. This suite did not contain all of the minor minerals found in the complex metamorphic rocks studied, which led to minor discrepancies in the model analysis, as discussed below, but did not affect the overall conclusions. All but three of the mineral spectra were obtained from the ASU Mineral Library. The spectra of sanidine, vesuvianite, and zoisite, measured in biconical reflectance, were obtained from *Salisbury et al*. [1991]. These spectra have been converted to emissivity assuming Kirchhoff's law ($\varepsilon = 1 - R$). This assumption is not strictly correct because these samples were measured in biconical, rather than hemispherical, reflection [*Salisbury et al*., 1994] but is adequate for the modeling performed here.

The spectral features of three minerals (serpentine, talc, and zoisite) were significantly shallower than spectral features observed in rocks containing these minerals. This is due to the presence of fine, clinging particles coating the mineral samples that are not present on the surfaces of minerals within rocks. These end-member spectra were scaled to approximate the rock spectra (Table 1). The spectra of three minor minerals (biotite, sanidine, and muscovite) were deeper than the features observed in average rock spectra. The sanidine spectrum was obtained from *Salisbury et al*. [1991], and its spectrum was adjusted to be consistent with the feldspar suite obtained in emission at ASU (Table 1). The spectra of biotite and muscovite were scaled to decrease their spectral contrast (Table 1) to a level more consistent with that observed in rocks. However, even with this adjustment, biotite and muscovite were difficult to identify, as discussed in sections 3.3 and 3.4.4.

Rock samples can have lower spectral contrast than the library minerals due to the large size (710–1000 μm) of the particles used for the library. In the application of this algorithm it has been observed that when the measured rock spectrum is significantly shallower than the combined mineral components the algorithm will use a relatively featureless mineral spectrum to compensate in the model. To limit this inappro-

Table 2. Rock Type and Sample Name of Samples Illustrated in Figure 1

Sample	Rock Type and Sample Name	Original Petrographic Analysis Source
ELF	hornblende-biotite granodiorite	*Borg et al*. [1986]
ENG	hornblende-biotite granodiorite	*Borg et al*. [1986]
ESM	quartz diorite	*Borg et al*. [1986]
EZS	biotite monzogranite	*Borg et al*. [1986]
BB2	Numbla Vale adamellite	*Chappell and White* [1976]
BB10	Buckely's Lake adamellite	*Chappell and White* [1976]
C1	Cooma granodiorite	*Chappell and White* [1976]
MG16	Tuross Head tonalite	*Chappell and White* [1976]
8218	latite	*Merrill* [1974]
8220	latite	*Merrill* [1974]
8234	quartz latite	*Merrill* [1974]
8235	rhyolite	*Merrill* [1974]
8236	alkali trachyte	*Merrill* [1974]
4-95-25	olivine-subalkali basalt	*Leighty* [1997]
9-94-12	basaltic andesite	*Leighty* [1997]
9-94-19	andesite	*Leighty* [1997]
9-94-36	basaltic andesite	*Leighty* [1997]
9-94-42	andesite	*Leighty* [1997]
12-94-8	basaltic andesite	*Leighty* [1997]
GM-1	albite-garnet-mica schist	S. Peacock (personal communication, 1997)
7047	phyllite	*Feely* [1997]
7461	retrograde sericite-mica phyllite	*Feely* [1997]
7471	phyllite	*Feely* [1997]
SC-15	vesuvianite-wollastonite granite	S. Peacock (personal communication, 1997)
7449	wollastonite marble	*Feely* [1997]
7573	tremolite marble	S. Peacock (personal communication, 1997)
7732	calc shist	*Feely* [1997]
Z-65	hornblende-biotite schist	S. Peacock (personal communication, 1997)
83-20	antigorite serpentinite	*Peacock* [1985]
83-47D	serpentinite	*Peacock* [1985]
86-10B	garnet-hornblende-diopside granofel	S. Peacock (personal communication, 1997)
7561	greenstone	*Feely* [1997]
7265	gneiss	*Feely* [1997]
7614	kyanite quartzite	*Feely* [1997]
14611	coarse banded gneiss	*Feely* [1997]
14613	augen granitegneiss	*Feely* [1997]

priate mineral identification, a blackbody spectrum, which has unit emissivity at all wavelengths, was also provided as a potential end-member [*Hamilton et al*., 1997; *Ruff*, 1998]. The blackbody abundances required to fit the spectra were generally small (<15%), which indicates that there is little decrease in the spectral contrast of rocks relative to coarse-grained mineral samples. Models containing blackbody as a component were normalized to adjust for the blackbody abundance before final analysis (i.e., a model that contains 53% quartz, 30% feldspar, and 17% blackbody, for a total of 100%, was normalized to 64% quartz and 36% feldspar).

3. Results and Discussion

3.1. Mineral Identification and Abundance

The spectra of all 96 rocks used in this study were analyzed using the linear deconvolution algorithm to identify the component minerals and their volume abundances. Examples of the fit of the model to the measured spectra are given in Figure 1 for a subset of 36 rock samples. The igneous samples range in composition from granodiorite (ELF) to basaltic-andesite (9-94-12) to rhyolite (8235), and the metamorphic samples were selected to cover a similarly representative range (see Table 2 for sample names and sources of the original petrographic analyses). The samples in Figure 1 were chosen to include examples of the best and worst model fits.

As seen in Figure 1, a linear model generally provides an excellent fit to the measured rock spectrum for a wide range of spectral shapes and rock compositions. Spectra with significant spectral detail and band depth (e.g., samples ELF, BB10, C1) are matched well. Spectra with broad features and reduced modulation of the fine-scale structure (e.g., samples MG16, 9-94-12, 9-94-36) are also closely matched by linear mixtures of end-member minerals. The formal error in the fit between the model and the original spectrum is given by the RMS emissivity error. Table 3 shows the RMS error by rock type, averaged for all of the samples, using the full suite of 36 end-member minerals with no initial assumption about the rock composition ("blind application"). The RMS difference between the model and measured spectra was 0.004–0.005 for igneous rocks and 0.008–0.014 for metamorphic rocks.

Figures 2 and 3 summarize the comparison of the mineral abundances determined spectroscopically and petrographically for all 96 rock samples. Data points that fall on the diagonal line represent a perfect agreement between the two techniques. Overall the spectroscopic analysis produces mineral abundances that agree well with the actual mineral abundances in each rock. We have attempted to quantify the uncertainties in the derived mineral abundances using the median and standard deviation of the differences in the mineral percentages derived from spectroscopic and petrographic techniques for the primary and secondary minerals.

The median value (Table 4) provides a measure of the systematic differences between the spectroscopic and petrographic methods. Only biotite + chlorite shows a significant systematic bias between the two techniques, with the spectro-

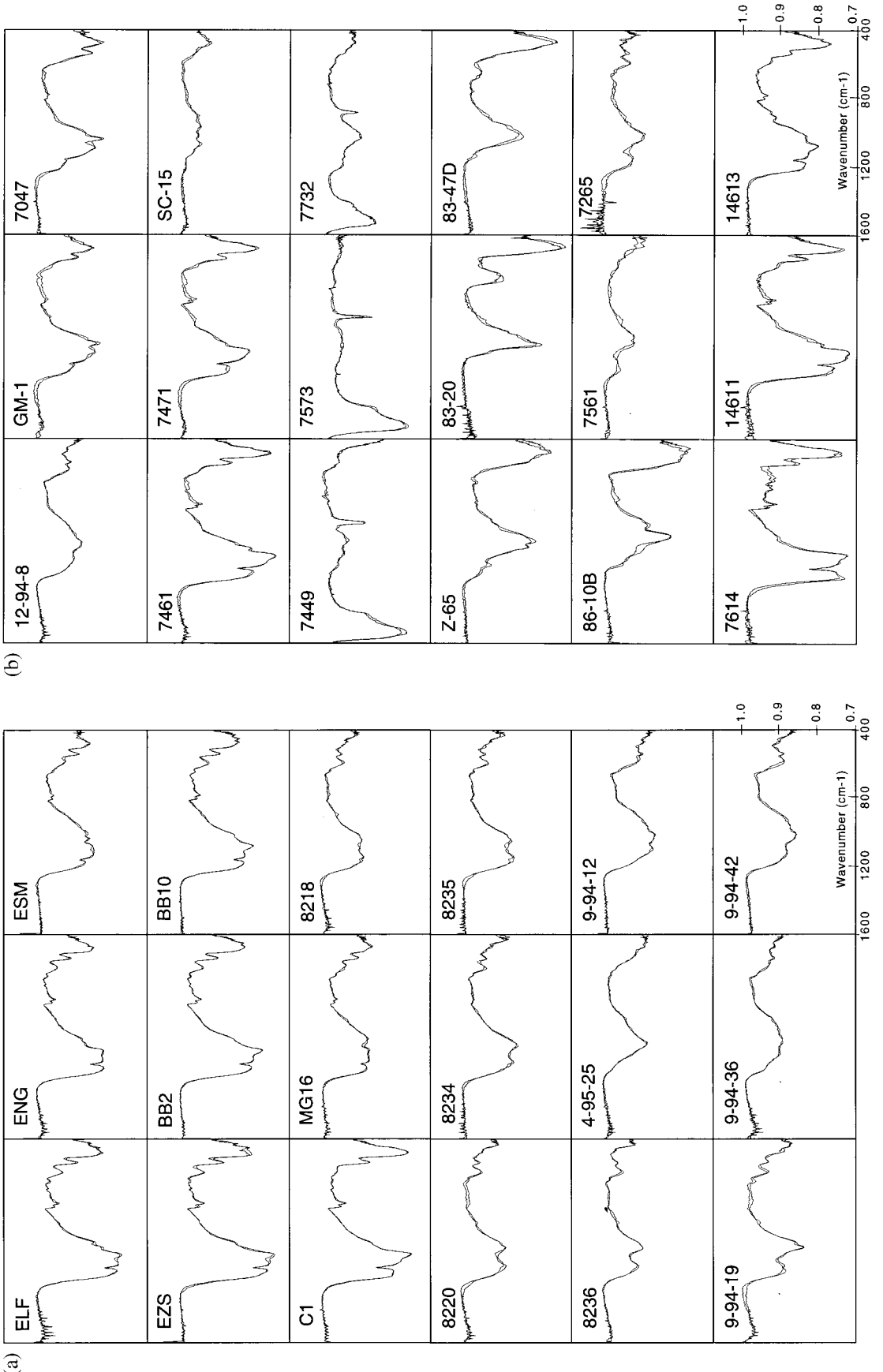

Figure 1. Examples of measured and model spectra for 36 igneous and metamorphic samples. Sample names and sources are given in Table 2. Each block plots wavenumbers (1600–400 cm^{-1}) along the x axis and emissivity (0.70–1.08) along the y axis. These spectra and model fits are reproduced from *Feely* [1997].

Table 3a. Comparison of RMS Error Results Using Blind and Controlled End-Member Suites

Rock Types	Blind Application	Controlled Application	Difference (Controlled Minus Blind)
Igneous			
Granite	0.0051	0.0060	0.0009
Rhyolite-andesite	0.0044	0.0055	0.0011
Basalt	0.0041	0.0056	0.0015
Metamorphic			
Pelite	0.0082	0.0100	0.0018
Calcareous	0.0108	0.0109	0.0001
Mafic	0.0142	0.0131	−0.0004
Quartz-feldspathic	0.0078	0.0083	0.0005

scopic method tending to underestimate the abundance of these minerals. In order to provide some measure of the spread of the uncertainties we have also determined the standard deviation of the differences (Table 4), assuming that they have a normal distribution. The one-sigma standard deviation of the difference between the quartz abundances derived by the two models is ±11%, i.e., 66% of the derived values for quartz fall within ±10.9% of the known value, which agrees well with visual inspection of Figures 2 and 3. The feldspar abundances agree to within ±15%, calcite and/or dolomite abundances agree to within ±14%, and pyroxene abundances agree to within ±7%. The major mineral (>5%) abundances of igneous rocks are more accurately determined than those of the metamorphic rocks, with errors typically within ±5–10%.

Errors in the spectroscopic determinations are not the only source of uncertainty because errors also exist for the known modes. The errors in the petrographic determinations are dependent on the method used to determine the rock composition. Traditional thin section mode estimates typically quote accuracies of ±5–15% for major minerals and ≤5% for minor minerals. Modes obtained by counting several thousand points per sample slide or slab have accuracies ranging from <1 to 3% for major and minor minerals. The majority of the samples used in this study have known modes estimated from thin sections, with only 34 samples analyzed by point-counting methods. In order to test the effect of petrographic analysis errors on our results we determined the accuracies of the mineral determinations using only the rocks with point count data. Unfortunately, data were only available for the quartz and feldspar minerals in the granite and andesite samples. The agreement between the spectroscopic and petrographic determination did improve slightly using the point count data, with the standard deviation in the differences for quartz and feldspar improving to 6.4% and 7.1%, respectively.

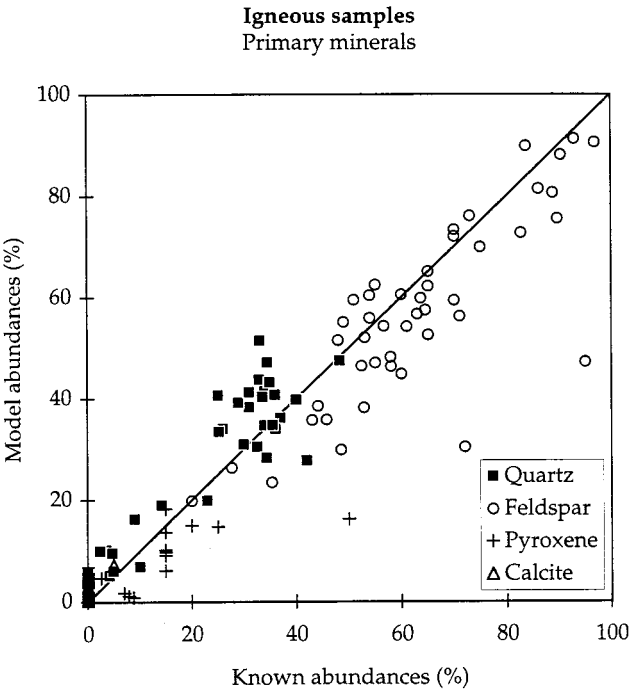

Figure 2. Comparison of petrographic and infrared modal analyses for quartz, feldspar, pyroxene, and calcite in igneous rock samples. The solid line represents a perfect match between the results of the two techniques. For the data shown, average deviation from the perfect match line ranges from ±2% to ±11%.

Another source of error in the known modes that is more difficult to quantify is due to human error when trying to differentiate between optically similar mineral species. This error is demonstrated by the results of sample 169, which was identified from hand sample and thin section analysis as a marble composed of ~75–100% calcite and 0–25% quartz [*Melchiorre*, 1993]. Deconvolution of the infrared spectrum indicated that the sample is 88% wollastonite, with only 4% calcite, 0% quartz, and trace amounts of garnet and talc (Figure 4). Further examination of the sample revealed that it is indeed almost entirely composed of wollastonite and does not react to hydrochloric acid. To our knowledge, this is the only

Table 3b. Comparison of Composition Error Results Using Blind and Controlled End-Member Suites

Minerals	Controlled Application		Blind Application		Difference (Standard Deviation) (Controlled Minus Blind)
	Standard Deviation	Median	Standard Deviation	Median	
Primary					
Calcite/dolomite	9.61	1.66	13.41	2.20	−3.80
Feldspar	15.40	−2.28	15.21	−2.47	0.19
Pyroxene	9.21	0.69	6.77	2.05	2.44
Quartz	11.88	0.78	10.93	1.08	0.95
Secondary					
Amphibole	13.51	−0.70	16.75	0.33	−3.24
Biotite/chlorite	10.28	−5.50	15.69	−7.50	−5.41
Muscovite	8.66	1.68	8.72	0.95	−0.06

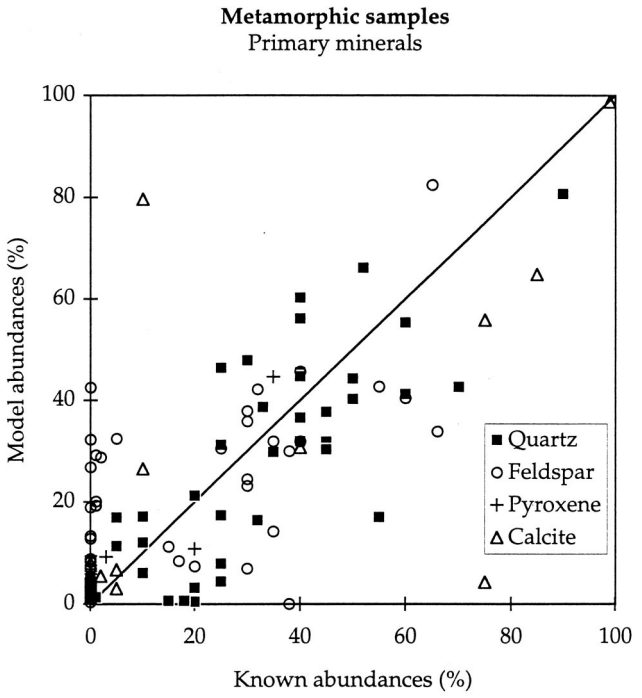

Figure 3. Comparison of petrographic and infrared modal analyses for quartz, feldspar, pyroxene, and calcite in metamorphic rock samples. These data are slightly more dispersed than the igneous data and show an average deviation from the perfect match line ranging from ±4% to ±19%.

sample used that contained a major error in the "known" modal analysis.

The results presented in Figures 2 and 3 are relevant to laboratory, field, and remotely sensed data with high spectral resolution (2–10 cm^{-1}) and broad wavelength coverage 6–25 μm). Other applications of this technique will include the use of multispectral remotely sensed data for which the spectral resolution and range are significantly reduced. As a simple test to estimate the effects of spectral resolution and range on the ability to derive mineral abundance from spectral measurements, we degraded the rock and mineral library spectral to simulate a 10-band multispectral instrument. The spectra were convolved with idealized square-wave filters 1 μm wide on 1 μm centers from 5.5 to 14.5 μm. These data were reanalyzed in a manner identical to that used for the data shown in Figure 2. Because there were only 10 bands, only 10 mineral end-

Table 4. Comparison of Modeled and Known Mineral Percentages

Mineral	Median Difference, %	Standard Deviation of Difference, %
Primary		
Calcite/dolomite	2.20	13.41
Feldspar	−2.47	15.21
Pyroxene	2.05	6.77
Quartz	1.08	10.93
Secondary		
Amphibole	0.33	16.75
Biotite + chlorite	−7.50	15.69
Muscovite	0.95	8.72

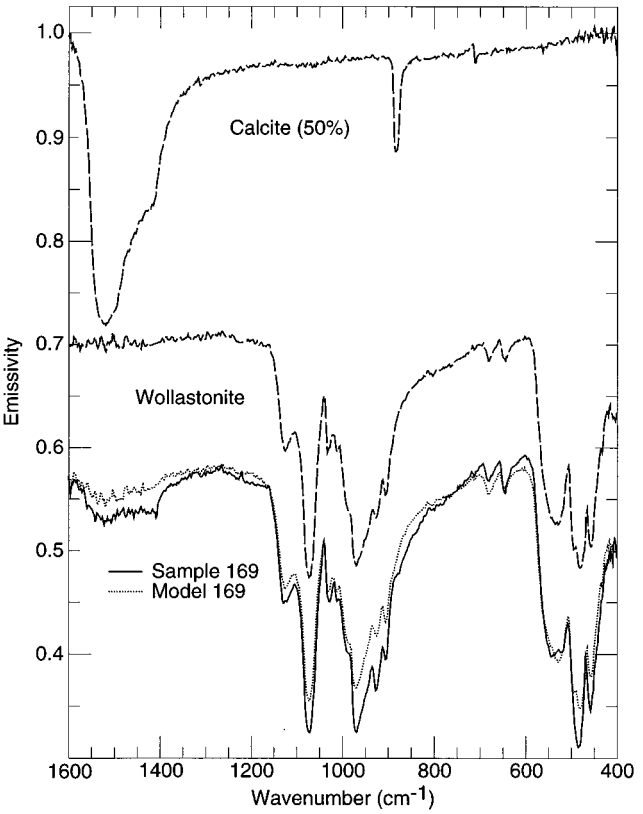

Figure 4. Comparison of calcite and wollastonite endmember spectra as potential constituents of sample 169, Precambrian marble. Deconvolution model is composed of 4% calcite, 88% wollastonite, and a few accessory minerals. Spectra are offset for clarity; wollastonite by −0.3, sample 169 and model 169 by −0.42.

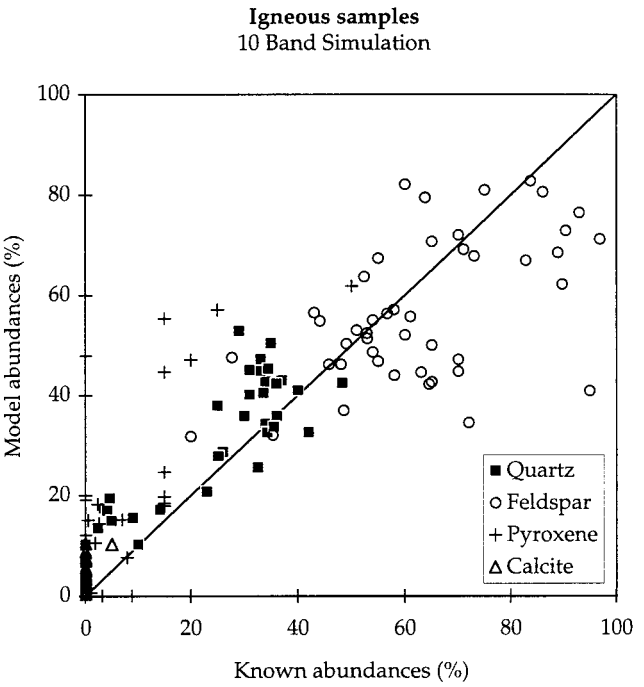

Figure 5. Comparison of petrographic and infrared modal analyses for the igneous rock suite after degrading the rock and mineral library spectra to simulated 10-band spectra.

members were used in the deconvolution. We selected calcite, three feldspars (microcline, albite, and anorthite), olivine, two pyroxenes (augite and diopside), quartz (slab and granular), and blackbody from the full library for use in the reduced end-member subset.

The comparison of the mineral abundances determined spectroscopically and petrographically for the igneous rock samples is shown in Figure 5 for the simulated 10-band spectra. As seen in Figure 5, the results are remarkably good considering the significant degradation applied to the spectra. All of the minerals present were successfully identified. Furthermore, the number of cases in which minerals were identified in the spectra that were not identified petrographically was unchanged. There is little change in the derived quartz abundance, and calcite was successfully identified. The pyroxene abundances were overestimated by up to ~30%, and the feldspar abundances were underestimated by comparable amounts.

Specific examples of the spectroscopic and petrographic mineral analyses are given for three rock samples in Table 5. Sample C1 is primarily composed of quartz, feldspars, biotite, and muscovite. Of these components the model accurately identified quartz, feldspar, and muscovite. Biotite was underestimated in the model and replaced by an assortment of accessory minerals, each identified at <4% for a total of 15.4%. This type of substitution for biotite with other minerals at low percentages occurs in many samples but can be reduced by using an igneous, felsic mineral end-member suite, rather than the general igneous and metamorphic end-member suite, as discussed below. A small amount of calcite was incorrectly identified to model the water vapor features at 1600–1400 cm^{-1}. The model produced by deconvolution matches the measured spectrum well with an RMS emissivity error of 0.0026.

Table 5. Modal Results for Selected Samples

Minerals	Known	Model
Sample C1, Cooma Granodiorite		
Biotite	17.4	7.16
Calcite	0.0	0.07
Garnet	0.0	0.32
Glass	0.0	2.20
Hornblende	0.0	2.68
K-feldspar	8.8	8.22
Muscovite	4.0	3.37
Olivine	0.0	2.54
Plagioclase	18.9	18.65
Pyroxene	0.0	3.87
Quartz	48.3	48.31
Serpentine	0.0	2.27
Blackbody		4.25*
Sample 9-94-12, Basaltic-Andesite		
Feldspars	65	62.30
Garnet	0	0.87
Glass	0	8.93
Muscovite	0	5.70
Olivine	5	5.07
Pyroxene	25	14.70
Quartz	0	0.53
Zoisite	0	2.10
Sample 86-10B, Garnet-Hornblende-Diopside Granofel		
Calcite	0	2.64
Epidote	0	9.89
Garnet	40	9.86
Hornblende	35	59.83
Olivine	0	5.54
Pyroxene	20	10.81
Quartz	1	1.30
Zoisite	0	0.46

* Normalized when blackbody present.

In some samples, such as granite, the spectral features of the dominant minerals (quartz and feldspars) are readily identifiable in the rock spectrum. However, many rock spectra are more complex mixtures of spectral features, and the individual mineral spectra are more difficult to visibly identify. For example, fine-grained basaltic and andesitic igneous rocks have spectra with broad features and less spectral detail (e.g., samples 9-94-12 and 9-94-36 in Figure 1). Even these spectra, however, are composed of a unique mixture of component mineral spectra that can be retrieved using a linear deconvolution. This ability to deconvolve overlapping bands is the strength of the deconvolution analysis technique and allows the component minerals to be retrieved from a complex mixture to within the error limits.

The ability to deconvolve complex rock spectra with low high-frequency spectral structure is illustrated in Figure 6 for sample 9-94-12. Petrographic analysis identified this sample as a basaltic andesite, composed of a mafic matrix supporting 1-mm olivine phenocrysts and pinpoint-sized vesicles (5%) [*Leighty*, 1997; *Feely*, 1997]. The model reproduced the measured spectra with an RMS error of 0.0036 and identified the three dominant minerals, feldspar, pyroxene, and olivine, to within ±3–11% (Table 5). Figure 6 shows the composite model spectrum, along with the spectra of the end-member minerals, and illustrates how the fine-scale spectral structure of the individual minerals can overlap and be subdued in the rock spectrum. Samples such as this would be difficult to analyze using comparisons of individual spectral band shapes to those of individual minerals. However, the component minerals can be identified by a simultaneous, least squares solution for all minerals present in the rock. Thus, while the spectra of the basalts and andesites have broad spectral features, their spectra can be uniquely matched, and the correct mixture of the mineral components can be determined with the same accuracy as obtained for rocks in which the individual mineral features can be directly identified.

In addition to the quantitative accuracies of the compositional results obtained using deconvolution, the shape of the sample spectra and general identification of minerals also provide a wealth of information at the qualitative level. Even when the mineral shapes and depths are not perfectly matched, or when other mineral end-member complications arise (discussed below), the general rock composition can be determined if the overall spectral match is good. For example, sample 86-10B (Figure 1 and Table 5) was modeled by 60% hornblende, 11% pyroxene, 10% garnet, and 10% epidote, with minor amounts of olivine, calcite, quartz, and zoisite, to reproduce the measured spectrum with a relatively high RMS of 0.0099. This analysis indicates that the sample is mafic with some degree of metamorphism; however, the poor fit to several of the features indicates that at least some of the minerals composing this sample are not available in the end-member suite. The known identity and composition of this sample (Table 5) shows that three major minerals (hornblende, pyroxene, and garnet) were correctly identified and that it is a metamorphosed mafic rock.

Most of the samples used in this study can be grouped by rock type based on their spectral shapes (Figure 1), as noted by

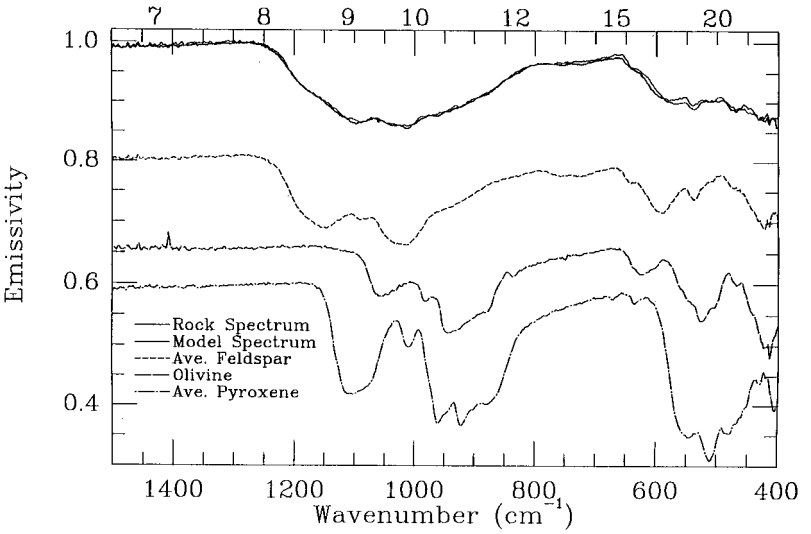

Figure 6. Measured and modeled spectra and the spectra of the major component minerals. The sample shown (9-94-12) is a basaltic andesite composed primarily of feldspar, pyroxene, and olivine (Table 5). While the component minerals have sharp, distinct spectral features from 8 to 12 μm, the rock spectrum has a broad shape in which the mineral spectral features are difficult to identify. The simultaneous, least squares deconvolution, however, provides an excellent fit to the rock spectrum and gives an accurate determination of the mineral composition and abundance as shown in Table 5. Spectra are offset for clarity; average feldspar by -0.2, olivine by -0.35, and average pyroxene by -0.4.

Hamilton et al. [1997] for mafic meteorites. Deep quartz features dominate most granitic, pelitic, and quartzo-feldspathic spectra (see sample C1 or 7614; Figure 1). Accessory metamorphic minerals in pelitic and quartzo-feldspathic samples contribute spectral features, especially at lower wavenumbers (longer wavelengths), that help differentiate some of these samples from their igneous equivalents. Fine-grained, feldspar-rich, igneous rocks have shallow spectra with a broad feature between 900 and 1200 cm^{-1}, usually occurring as distinct double absorptions in rhyolitic or andesitic samples (see sample 8236, Figure 1) or becoming broader due to the mafic minerals in basaltic samples (see sample 9-94-36, Figure 1). Compared to these igneous rocks, the metamorphosed mafic samples often have sharper features in these approximate wavelength regions due to the dominant features of the metamorphic mafic minerals superimposed over the feldspars (e.g., sample Z-65, Figure 1). Significant amounts of calcite or dolomite in a rock result in two deep features at 1400–1600 and 880 cm^{-1}, allowing easy identification of calcareous samples (see sample 7573, Figure 1).

3.2. "Blind" Versus "Controlled" Applications

The results included here for igneous and metamorphic rock samples represent a blind application of the deconvolution modal analysis technique, where a single end-member mineral suite was used to determine the composition of a wide range of rock samples. A different approach is presented in detail by *Feely* [1997], where the same modeling technique was applied except that separate end-member suites were used that contained only minerals common to the specific rock type being analyzed (granite, basalt, pelite, calcareous, etc.). Because some basic knowledge of the rock type of the sample is required prior to deconvolution in order to choose the most appropriate end-member suite, this type of analysis is a "controlled application." The blind application achieved slightly better model fits than the controlled method (lower RMS in Table 3a) because there were more potential minerals to use in the deconvolution. For example, many metamorphic secondary and accessory minerals, in both igneous and metamorphic models, were incorporated at abundances of $<5\%$ and provided improved matches to the subtle spectral structure (often noise) in the sample spectra. However, the blind method does not necessarily provide a more accurate determination of the rock composition. The improvements in compositional determination using the controlled method are illustrated in Table 3b. The controlled application gave somewhat ($\sim$4%) better results for calcite/dolomite and the secondary minerals but did not improve the results for the other minerals. On average, the difference between the abundances derived by the blind and controlled applications is $\leq 5\%$.

A combined technique, using results from a first blind application to tailor an end-member suite for a second controlled application analysis on the same sample, would incorporate the best attributes of the two approaches. The important assumption in this technique is that many minerals in the blind end-member suite are not actually present and that their removal results in an improved compositional analysis. Specific factors, such as a priori knowledge of the sample rock type, expectations for or against particular rock types in the sample area, or geologically unreasonable mineral assemblages proposed by the blind application, may support this assumption. Based primarily on the assumption of geologically plausible mineral suites, a simplified end-member suite, with 11 of the less common metamorphic accessory minerals removed, was used in a second controlled application with eight of the samples selected from this study. The results for each stage of the analysis are shown in Figures 7a and 7b. In general, the compositional results were only slightly improved. Nine minor minerals present in the rocks were successfully identified in the controlled application but not in the blind method. Eleven major minerals were identified with slightly greater (5–10%) accuracy

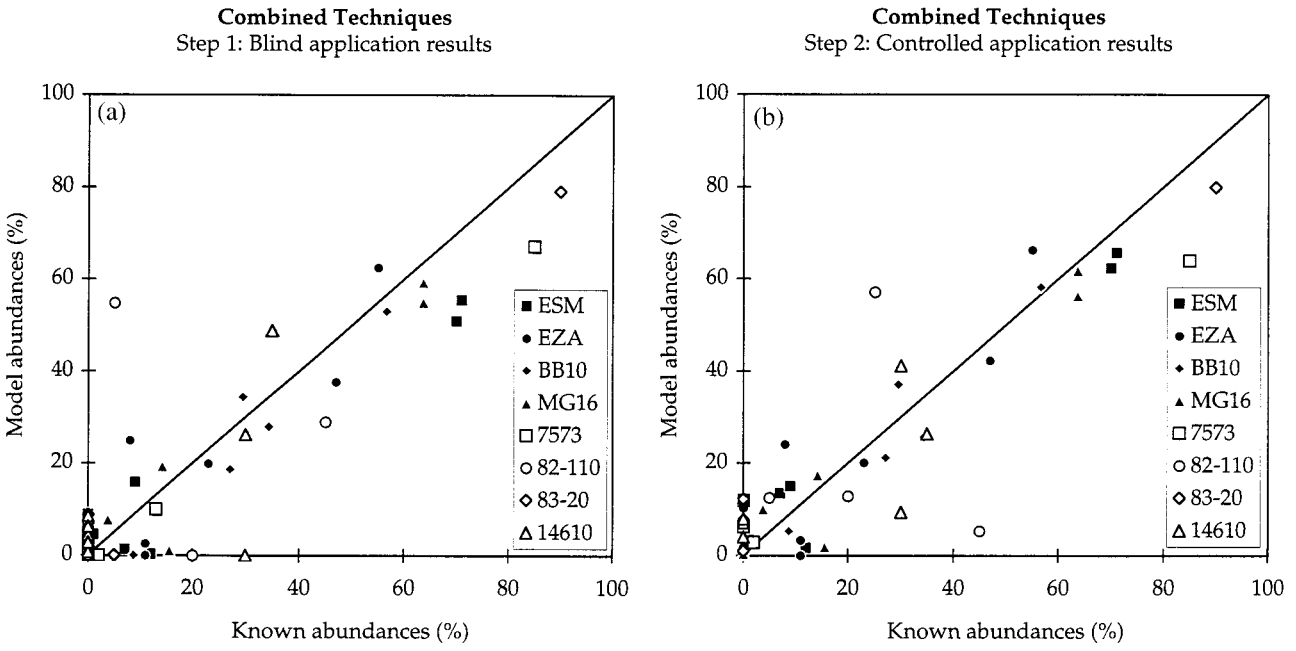

Figure 7. Infrared modal analyses are plotted against the petrographic composition for eight igneous and metamorphic samples. Each symbol represents the abundance for each mineral in a single rock. (a) Results from a blind application, using a general 36-mineral end-member suite. (b) Results of the controlled application, in which the results from Figure 7a were used to simplify the end-member suite to 26 minerals.

in the controlled technique, whereas three minerals were less accurately identified.

3.3. Detection Limits

The average detection limit of the deconvolution algorithm has been estimated to be 4.0% ± 0.5% [*Ramsey and Christensen*, 1998] based on extensive statistical evaluation of the algorithm and on the observation that minerals known to be present in abundances of about ≤5% contribute little to the overall measured spectrum of a rock sample. Therefore minerals that are modeled using the deconvolution algorithm at abundances of <5% may not actually be in the rock sample.

False identification or omission of mineral components in an infrared spectrum at the 5% level is not considered to be a serious problem for many applications because these minerals would constitute secondary and accessory minerals which are not usually necessary for rock identification. However, if many minerals are present with low individual abundances, together they may account for a significant proportion of the spectrum, and this could have repercussions on the features and component percentages of the model produced. Using the blind application, an average of two to four minerals per sample were identified at <5% (Figure 8) and account for an average of 8–9% (maximum 25%) of the total abundance. These false identifications resulted in a lowered model component of one of the known minerals, often feldspar or biotite in the rocks used in this study. Cases where there are large errors in the model abundances often had poor overall model fits. In several of these cases the errors are indicative of minerals present in the rock but not available in the end-member suite (see below).

Major accessory minerals that composed 10–20% of the known modal mineralogy, such as chlorite, sericite/white mica, and serpentine, were included in the end-member suite and were accurately identified during deconvolution. However, many of the metamorphic samples in this study also include minor (≤10%) amounts of one or more of the following: apatite, epidote, graphite, kyanite, rutile, sillimanite, sphene, spinel, tourmaline, zircon, zoisite, and unidentified opaques. Of these, only epidote, kyanite, and zoisite were available in the end-member suite. While these minerals were usually identified in models of samples where they are known to be present, they were often falsely identified at minor levels (≤5%) in models of samples where they were absent. Thus, even if the minor minerals were included in the end-member suite, it is not certain that the compositional matches for these minor minerals would improve.

Misidentification at the 5% level was higher during blind applications than controlled applications because of the number of minor and accessory minerals that were available to be incorporated into the best fit solution. While the use of minor amounts of these minerals improved the overall fits, these minerals often constitute "noise" in the compositional solution. In general, removal of those minerals that occur at low abundances from the end-member library did not significantly degrade the overall fit and gave a clearer picture of the major mineralogy of the sample.

3.4. Other Factors

3.4.1. Natural mineral variability. The minor deviations between the corresponding sample and model spectra are due in part to the inherent variability in the composition of naturally occurring minerals. Solid solution series minerals, such as feldspars (Figure 9) and pyroxenes, exhibit systematic shifts in the location of diagnostic spectral features [*Farmer*, 1974; *Nash and Salisbury*, 1991; *Salisbury et al.*, 1987; *Ruff*, 1998; *Hamilton*, 1998]. While the end-member suites incorporated a range of mineral compositions in the solid solution series, a complete suite of samples is not available. Vitrification and grain size can also play a role in varying spectral properties, such as demon-

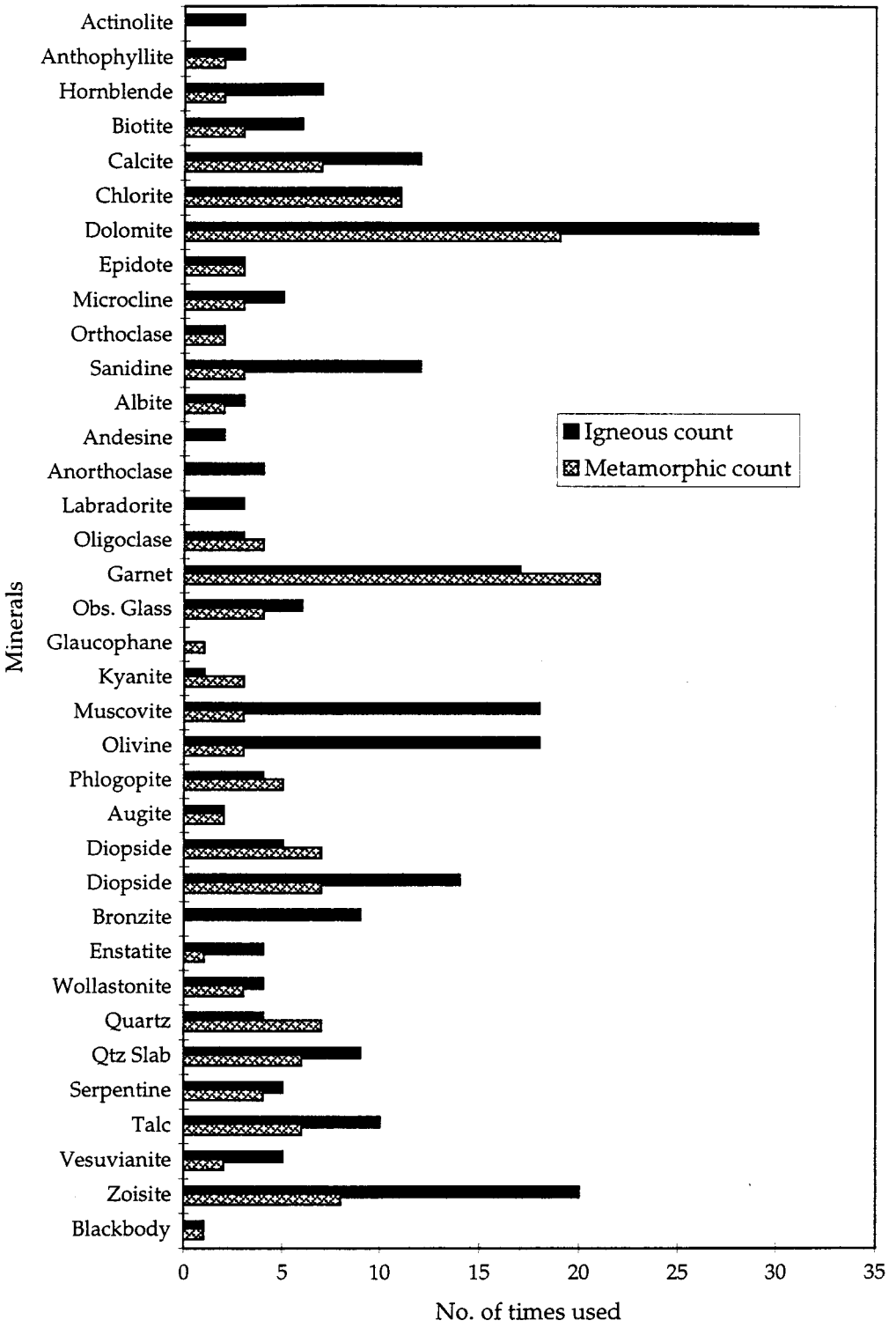

Figure 8. End-member minerals identified in models at abundances of ≤5%, near the limits of deconvolution accuracy. Histogram indicates that dolomite, garnet, muscovite, olivine, and zoisite are commonly used to model subtle features in the rock spectra, although their actual presence in the sample may be questionable.

strated for the plagioclase series by *Nash and Salisbury* [1991]. Therefore subtle differences can exist between the spectra of minerals in the rock samples and the spectra of the available end-member minerals. As a result of these differences, the sample spectra could not always be precisely matched.

In addition, the available petrographic data were often not sufficiently detailed to allow a comparison with the model abundances derived for different members of the solid solution series. Therefore all figures presented in this paper compare the total feldspar or pyroxene composition because the avail-

able known modes rarely distinguish between individual solid-solution members. Where detailed comparison was possible, deconvolution tended to slightly underestimate plagioclase abundances and slightly overestimate K-feldspar abundances, while maintaining a total feldspar composition that is within the experimental error stated above (Figure 10). This pattern is partially explained by the fact that K-feldspar has deep, distinct features, whereas the library spectra of the coarse-grained oligoclase, andesine, and anorthite samples have shallow, broad features (Figure 9). In general, when two end-members have similar spectral shapes, the one with the greater high-frequency spectral variation is preferentially selected because it can provide a better fit to the noise and other variability present in the spectrum [*Ruff*, 1998]. As a result, the K-feldspar minerals may be preferentially selected.

The shape, depth, and location of absorption features are also dependent on the exact crystal structure and atomic composition [*Lyon*, 1965; *Walter and Salisbury*, 1989; *Salisbury et al.*, 1991; *Salisbury*, 1993]. For example, subtle variations in mineral structure can account for the slight differences between the spectra of crushed crystalline quartz and a solid slab of vein quartz seen at 1190, 540, and 515 cm^{-1} and the depth of features between 790 and 700 cm^{-1}. Both of these samples were available in the mineral suite and were used individually or together in several model fits.

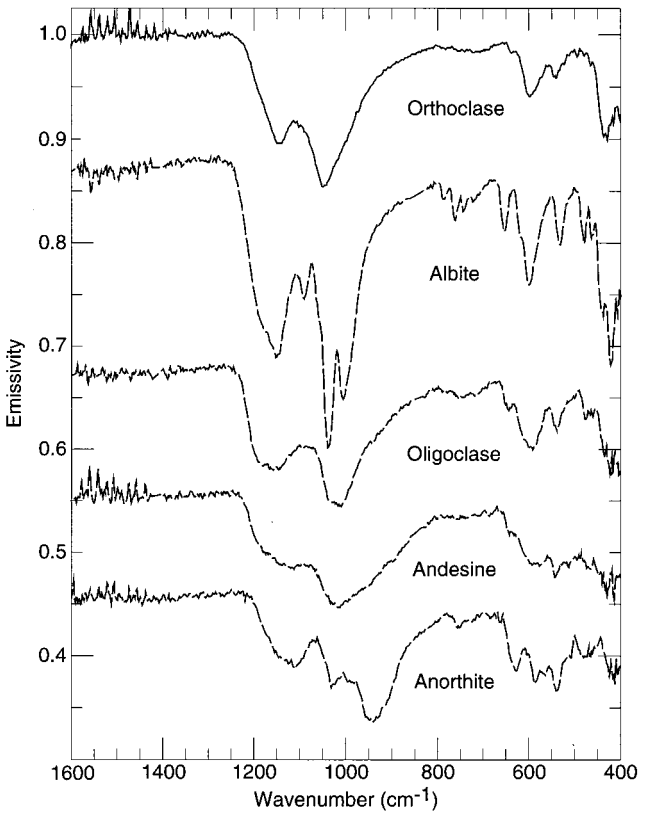

Figure 9. Several feldspar end-member spectra, including K-feldspar (top) and plagioclase solid solution series (bottom four). Variations in the shape and location of absorption features demonstrate effect of the changing composition from $KAlSi_3O_8$ (K-feldspar) and $NaAlSi_3O_8$ (albite) to $CaAl_2Si_2O_8$ (Anorthite). Spectra are offset for display; albite by −0.12, oligoclase by −0.32, andesine by −0.45, and anorthite by −0.54.

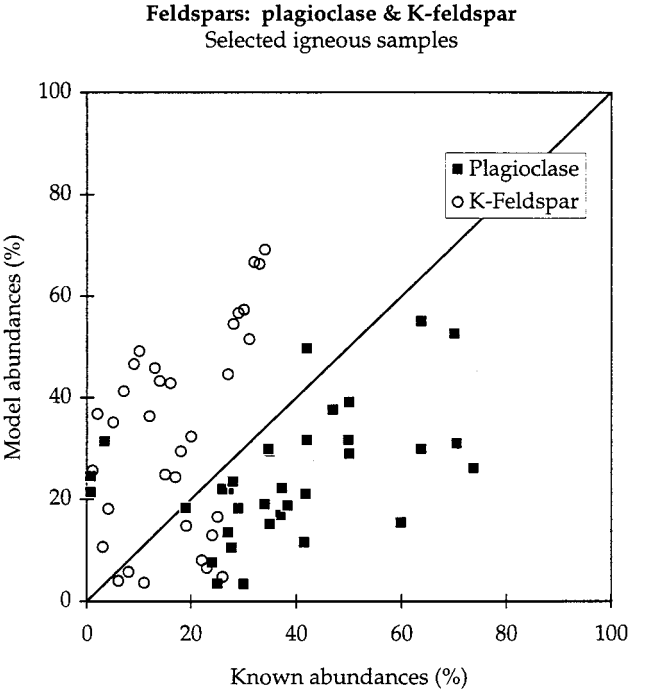

Figure 10. Comparison of modal analyses for plagioclase and K-feldspar in igneous samples for which differentiated petrographic modes are available. Plagioclase tends to be underestimated and K-feldspar tend to be overestimated, as indicated by the points below and above the perfect match line, respectively. When combined, the total feldspar composition is accurate to ±11% (see Figure 2).

3.4.2. Missing end-members. Figure 11 illustrates two examples (sample 7805, a spurrite hornfels, and sample 7709, a glaucophane schist) of how the algorithm responds when a major component is not available as an end-member. The composition of the spurrite hornfels is 90% spurrite (unavailable) and 10% calcite, but it was modeled with a combination of available end-members: feldspar, calcite, garnet, olivine, and wollastonite. The RMS error in this sample is relatively high (0.0139), and visual inspection confirms a poor fit (Figure 10). The glaucophane schist is composed of 60% glaucophane, 25% lawsonite (unavailable), and 10% quartz, but was modeled with feldspar, glaucophane, and quartz and minor (<10%) amounts of amphibole, chlorite, garnet, kyanite, olivine, pyroxene, vesuvianite, and blackbody. Again, the RMS error was relatively high (0.0064).

These samples demonstrate that when an end-member is not present in the library, a sample generally cannot be fit well by some combination of the end-members present. These results provide additional insight into the uniqueness of the sample compositions determined from spectral analyses. If the correct minerals are not present in the library, then the samples studied could not be fit well by any combination of available end-members. Conversely, good model fits, determined both by the RMS error and by visual inspection, are strong indicators that the correct minerals in the correct abundances have been accurately determined. The deconvolution results for these two samples also indicate that complex models that predict unlikely or geologically impossible mineral associations are a good indication that an important mineral is absent from the end-member suite.

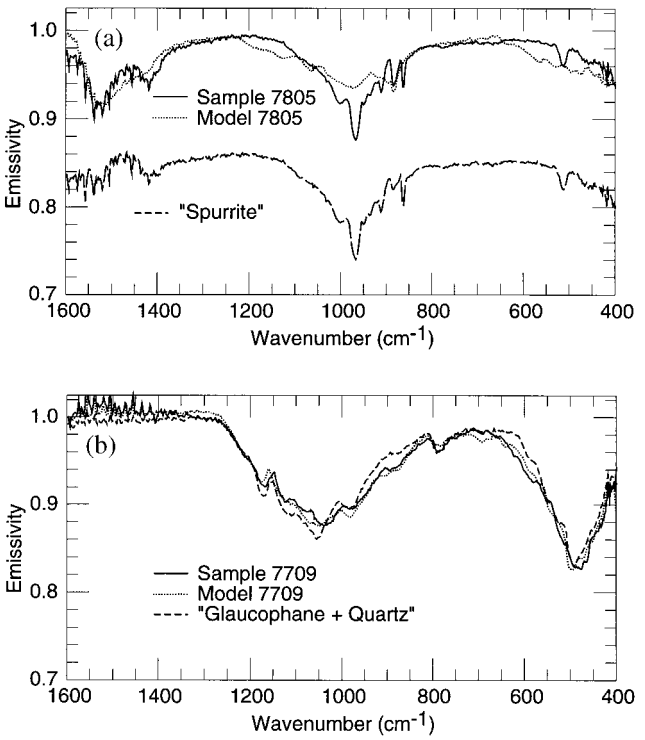

Figure 11. Examples of deconvolution results with incomplete end-member suites. (a) Derived "spurrite" mineral spectrum with sample and deconvolution model spectra for spurrite hornfels, sample 7805 (RMS = 0.0139). Spectra offset for display. (b) Sample 7709, glaucophane schist with deconvolution model and spectrum synthesized from glaucophane and quartz (RMS = 0.0064).

3.4.3. Calcite and dolomite. Calcite and dolomite are often intergrown and were frequently identified as a single "calcareous" component in optical modal analyses. Although they are easily distinguished spectrally, the model abundances were combined to allow for comparison with the less precise petrographic determinations. Calcite or dolomite was identified in 47 samples at $\leq 5\%$ (Figure 8) with no reported calcareous component. In five samples, calcareous weathering and alteration products were subsequently observed, and the spectral identification was accurate. In at least 30 other samples, calcareous minerals were incorrectly fit to water-vapor absorption features at 1400–1600 cm^{-1}. For abundances $>5\%$ the presence of carbonate, rather than water vapor, could be confirmed using the 880 cm^{-1} carbonate band. In the remaining 12 samples it is not known whether or not carbonates were actually present.

3.4.4. Biotite, chlorite, muscovite. Misidentification was commonly observed in the mica group (biotite, chlorite, muscovite). Even after decreasing the depth of spectral features in biotite and muscovite (Table 1), the abundance of these minerals is consistently underestimated. For at least 10 samples the deconvolution model used a chlorite component, which has a similar spectrum (Figure 12), instead of biotite, the mineral known to be present. This indicates either that the additional features between 600 and 800 cm^{-1} made chlorite a more suitable component for those samples or that more biotite had altered to chlorite than was identified in the petrographic studies.

In general, modes for all micas were underestimated with respect to the known modes in igneous samples and ranged widely from underestimated to overestimated in metamorphic samples. The majority ($\sim 80\%$) of the petrographically identified biotite + chlorite in igneous samples was not recognized during deconvolution. Examination of several of the granite samples known to contain 0–10% biotite + chlorite reveals that none of the characteristic spectral features can be observed. This indicates that the problem is not due to inaccurately identifying mica features as another mineral, but rather the problem is due to a difficulty of measuring biotite + chlorite abundances of $<10\%$ in a rock spectrum. Falsely identified muscovite averages $\sim 4\%$ and occurs most often in andesitic to basaltic igneous samples, most of which are characterized by shallow spectra, with broad features and/or glass features. These observations suggest that the limit of detection is 10% for all micas (Table 4).

3.4.5. Amphiboles. Amphiboles are a second group of minerals that are difficult to model accurately. They were often overestimated during deconvolution of metamorphic samples, with abundances up to 40% when there is no corresponding known abundance, and underestimated in igneous samples with known abundances of up to 11%. These errors are indicative of a combination of effects: the overestimation results from the use of amphibole, like a few of the other secondary metamorphic minerals, to fit features in the sample spectrum not accounted for by the other end-members. The deficiency of amphiboles in igneous samples may be due to overlaps in the characteristic spectral features, making it difficult to identify

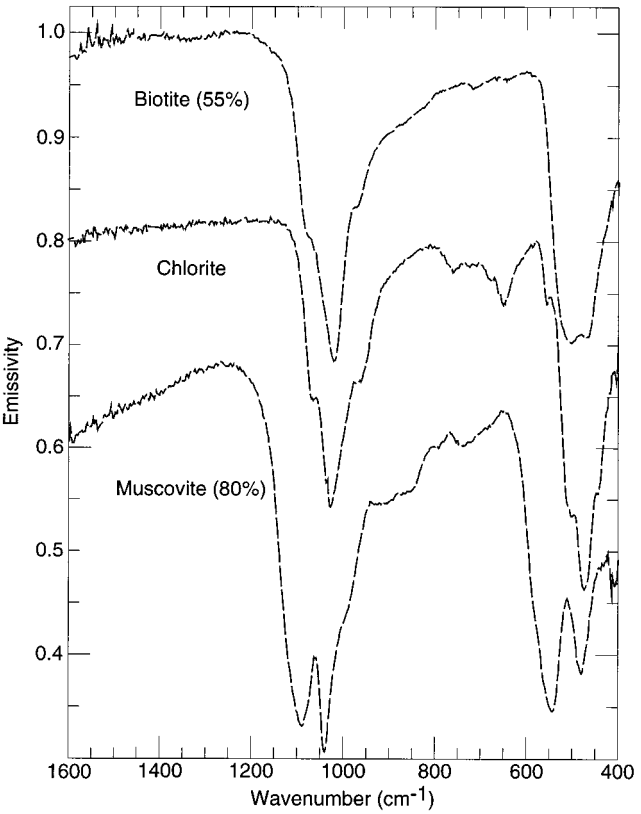

Figure 12. Chlorite and artificially shallowed biotite and muscovite spectra. Note the similarity of the position and shape of the biotite and chlorite spectral features. Spectra offset for display; chlorite by −0.2 and muscovite by −0.33.

amphiboles at <10% abundance. These observations suggest that the limit of detection is ±15–20% for the amphiboles and that there is a tendency for linear deconvolution to overestimate amphiboles in metamorphic samples (Table 4).

3.4.6. Metamorphic foliation. Variable degrees of foliation in 21 of the 51 metamorphic samples caused minor variations in the spectra measured at different sample orientations, which could have implications on the results of the compositional analysis. Spectra were obtained from sample surfaces oriented both normal to and along the foliation direction. The mineral composition results shown in Figure 3 were obtained by deconvolving the average spectrum of all available orientations. Most of the variation between oriented spectra was observed as deeper absorption features, with little change in the overall spectral shape. For a few of the samples, mica features, primarily located between 1000 and 1100 cm^{-1}, were enhanced when the sample was viewed perpendicular to the foliation. Thus *Lyon and Burns* [1963] were correct in their prediction that foliated rocks would show preferential orientation effects; however, the differences were not significant enough to warrant additional consideration during this study.

4. Conclusions

A deconvolution technique has been applied to determine the quantitative mineral composition of igneous and metamorphic rocks from their infrared spectrum based on the hypothesis that a measured rock spectrum represents a weighted linear summation of the mineral spectra that compose the sample. A compositional analysis of each sample derived from deconvolution of the infrared spectrum was compared with the petrographically estimated modes for each sample.

From the results presented here, the following conclusions can be drawn:

1. Linear mixing is a valid assumption for infrared emission spectra of rocks, and deconvolution of an infrared spectrum can be used to determine the quantitative mineral composition of rock samples. The deconvolution model successfully identified the mineral composition of 96 samples using an end-member spectral library of 36 common rock-forming and accessory minerals. Spectroscopically determined modal compositions are accurate to ±0–15% for the major minerals of quartz, feldspar, pyroxene, and calcite/dolomite and accurate to ±0–17% for minor minerals including micas and amphiboles. These values are comparable to the error for traditional thin section mode estimates, usually quoted as ±5–15% for major minerals and ≤±5% for minor minerals. They are less accurate than the results obtained by point counting several thousand points per sample, which typically range from <1 to 3% for major and minor minerals.

2. Lack of the correct end-members in the library results in a poor model fit. This observation supports the uniqueness of the model fits by demonstrating that good fits cannot be obtained by a fortuitous combination of incorrect spectra.

3. The detectability limits of the technique as applied here are ~5% for most minerals, increasing to ~10% for micas and ~15% for amphibole secondary minerals.

4. Each major rock type studied here is easily distinguished by its spectral characteristics. The best results, in both the qualitative recognition of the basic rock type and dominant minerals and in the quantitative reproduction of absorption features and mineral composition, were obtained for igneous rock samples. For metamorphic rocks the reproducibility and compositional analysis of the pelite and quartzo-feldspathic samples were slightly better than for calcareous or mafic samples.

5. Knowledge of the approximate rock type is not necessary before deconvolution is applied to the sample spectrum, and accurate compositional analysis can be conducted with a general mineral suite. If desired, these results can be used to simplify the end-member suite in a second analysis and obtain slightly more accurate results. However, these specialized end-member suites only improved the results by a few percent for most primary and secondary minerals. Thus a blind application is more robust because it requires no a priori knowledge of the sample, and it give comparable results to a more restricted suite of specific minerals.

6. The main challenges encountered in the deconvolution modal analysis technique are (1) the identification of true mineral constituents with abundances near the detectability limits of the technique and (2) the inclusion all of the potential mineral constituents included in the end-member suite.

The analysis procedure developed here can be used for modal analysis of hand samples from a geologic field study, either in lieu of traditional petrographic methods or to assist with the distinction between optically similar species. With the rapid advances in technology, portable field-size spectrometers and laptop computers will make this a valuable technique for compositional analysis of rocks in the field.

Acknowledgments. We would like to acknowledge the work of S. Ruff in developing the ASU spectroscopy lab used to acquire the emission spectra used here; J. Bandfield, V. Hamilton, M. Lane, J. Piatek, and S. Ruff for the development of the ASU Mineral Library used in this work; S. Borg, B. Chappel, R. Leighty, R. Merril, S. Peacock, and B. White for providing samples and petrographic analyses; and S. Peacock for assistance in the acquisition and analysis of additional rock samples. V. Hamilton, J. Moersch, and an anonymous reviewer provided helpful reviews that substantially improved this manuscript. This work was supported by a grant from the NASA Geology and Geophysics Program.

References

Adams, J. B., M. O. Smith, and P. E. Johnson, Spectral mixture modeling: A new analysis of rock and soil types at the Viking Lander 1 site, *J. Geophys. Res*., *91*, 8098–8112, 1986.

Borg, S. G., E. Stump, and J. R. Holloway, Granitoids of Northern Victoria Land, Antarctica: A reconnaissance study of field relations, petrography, and geochemistry, in *Geologic Investigations in Northern Victoria Land*, *Antarct. Res. Ser*., vol. 46, edited by E. Stump, pp. 115–118, AGU, Washington, D. C., 1986.

Chappell, B. W., and A. J. R. White, *Plutonic Rocks of the Lachlan Mobile Zone*, *Field Excursion Guide 13C*, 25th Int. Geol. Congr., Sydney, Australia, 1976.

Christensen, P. R., and S. T. Harrison, Thermal infrared emission spectroscopy of natural surfaces: Application to desert varnish coatings on rocks, *J. Geophys. Res*., *98*, 19,819–19,834, 1993.

Christensen, P. R., J. L. Bandfield, V. E. Hamilton, D. A. Howard, M. D. Lane, J. L. Piatek, S. W. Ruff, and W. L. Stefanov, A thermal emission spectral library of rock-forming minerals, *J. Geophys. Res*., in press, 1999.

Conel, J. E., Infrared emissivities of silicates: Experimental results and a cloudy atmosphere model of spectral emission from condensed particulate mediums, *J. Geophys. Res*., *74*, 1614–1634, 1969.

Farmer, V. C., *The Infrared Spectra of Minerals*, 539 pp., Mineral. Soc., London, 1974.

Feely, K. C., Quantitative compositional analysis of igneous and metamorphic rocks using infrared emission spectroscopy, Masters thesis, Ariz. State Univ., Tempe, 1997.

Hamilton, V. E., Thermal infrared emission spectroscopy of the py-

roxene mineral series and pyroxene-bearing lithologies, Ph.D. dissertation, Ariz. State Univ., Tempe, 1998.
Hamilton, V. E., P. R. Christensen, and H. Y. McSween Jr., Determination of martian meteorite lithologies and mineralogies using vibrational spectroscopy, *J. Geophys. Res*., *102*, 25,593–25,603, 1997.
Hunt, G. R., and R. K. Vincent, The behavior of spectral features in the infrared emission from particulate surfaces of various grain sizes, *J. Geophys. Res*., *73*, 6039–6046, 1968.
Hunt, J. M., and D. S. Turner, Determination of mineral constituents of rocks by infrared spectroscopy, *Anal. Chem*., *25*, 1169–1174, 1953.
Johnson, P. E., M. O. Smith, and J. B. Adams, Simple algorithms for remote determination of mineral abundances and particle sizes from reflectance spectra, *J. Geophys. Res*., *97*, 2649–2657, 1992.
Leighty, R., Neogene tectonism and magmatism across the Basin and Range–Colorado Plateau boundary, central Arizona, Ph.D. dissertation, Ariz. State Univ., Tempe, 1997.
Lyon, R. J. P., Evaluation of infrared spectrophotometry for compositional analysis of lunar and planetary soils, final report, Stanford Res. Inst., Menlo Park, Calif., 1963.
Lyon, R. J. P., Analysis of rocks by spectral infrared emission (8–25 microns), *Econ. Geol*., *60*, 715–736, 1965.
Lyon, R. J. P., and E. A. Burns, Analysis of rocks by reflected infrared radiation, *Econ. Geol*., *58*, 274–284, 1963.
Lyon, R. J. P., W. M. Tuddenham, and C. S. Thompson, Quantitative mineralogy in 30 minutes, *Econ. Geol*., *54*, 1047–1055, 1959.
Melchiorre, E. B., Proterozoic geology of the Sierra Estrella, Arizona, Master's thesis, Ariz. State Univ., Tempe, 1993.
Merrill, R. K., The Late Cenozoic geology of the White Mountains, Apache County, Arizona, Ph.D. dissertation, Ariz. State Univ., Tempe, 1974.
Nash, D. B., and J. W. Salisbury, Infrared reflectance spectra of plagioclase feldspars, *Geophys. Res. Lett*., *18*, 1151–1154, 1991.
Peacock, S. M., Thermal and fluvial evolution of the Trinity thrust system, Klamath Province, northern California: Implications for the effect of fluids in subduction zones, Ph.D. dissertation, Univ. of Calif., Los Angeles, 1985.
Ramsey, M. S., and P. R. Christensen, Mineral abundance determination: Quantitative deconvolution of thermal emission spectra, *J. Geophys. Res*., *103*, 577–596, 1998.
Ramsey, M. S., J. H. Fink, and P. R. Christensen, Thermal emission analysis of mineral glasses: Application to remote sensing studies of Holocene silicic laval flows, paper presented at General Assembly IAVCEI, 1993.
Ruff, S. W., Quantitative thermal infrared emission spectroscopy applied to granitoid petrology, Ph.D. dissertation, Ariz. State Univ., Tempe, 1998.
Ruff, S. W., P. R. Christensen, P. W. Barbera, and D. L. Anderson, Quantitative thermal emission spectroscopy of minerals: A technique for measurement and calibration, *J. Geophys. Res*., *102*, 14,899–14,913, 1997.
Salisbury, J. W., Mid-infrared spectroscopy: Laboratory data, in *Remote Geochemical Analysis: Elemental and Mineralogical Composition*, edited by C. Pieters and P. Englert, pp. 79–98, Cambridge Univ. Press, New York, 1993.
Salisbury, J. W., L. S. Walter, and N. Vergo, Mid-infrared (2.1–25 μm) spectra of minerals, 1st ed., *U.S. Geol. Surv*., *Open File Rep*., *87-263*, 1987.
Salisbury, J. W., L. S. Walter, N. Vergo, and D. M. D'Aria, *Infrared (2.1–25 μm) Spectra of Minerals*, 267 pp., Johns Hopkins Univ. Press, Baltimore, Md., 1991.
Salisbury, J. W., A. Wald, and D. M. D'Aria, Thermal-infrared remote sensing and Kirchhoff's law, 1, Laboratory measurements, *J. Geophys. Res*., *99*, 11,897–11,911, 1994.
Thomson, J. L., and J. W. Salisbury, The mid-infrared reflectance of mineral mixtures (7–14 μm), *Remote Sens. Environ*., *45*, 1–13, 1993.
Vincent, R. K., and F. Thompson, Spectral compositional imaging of silicate rocks, *J. Geophys. Res*., *77*, 2465–2472, 1972.
Walter, L. S., and J. W. Salisbury, Spectral characterization of igneous rocks in the 8–12 μm region, *J. Geophys. Res*., *94*, 9203–9213, 1989.
Wilson, E. B., Jr., J. C. Decius, and P. C. Cross, *Molecular Vibrations: The Theory of Infrared and Raman Vibrational Spectra*, McGraw-Hill, New York, 1955.

P. R. Christensen and K. C. Feely, Department of Geology, Campus Box 871404, Arizona State University, Tempe, AZ 85287-1404. (phil.christensen@asu.edu)

(Received February 23, 1999; revised June 18, 1999;
accepted June 22, 1999.)